Near-exit flow-field investigation in an inducer including laser-Doppler velocimetry

J. H. G. Howard and A. Atif
Mechanical Engineering Department, University of Waterloo, Waterloo, Ontario, Canada

The flow field was measured near the exit of an axial-flow spiral-inducer pump impeller at design and off-design conditions. Laser-Doppler velocimetry was employed to define the blade-to-blade velocity distribution inside and outside the rotating impeller passage near the trailing edge. The observed variation of velocity and flow angle revealed a strong secondary flow, of a double vortex form, at the design flow rate and a developing hub separation zone at lower flow rates. The observed rearrangement of the flow field between the closely spaced locations upstream and downstream of the trailing edge is believed to be linked to the developing recirculation zone. Distributed deviation angles are presented for the design flow rate and overall values for all flow rates.

Keywords: internal flow field; inducer; axial-flow pump; secondary flow

Introduction

Some pumps employ an axial-flow spiral inducer to handle cavitating or two-phase flow. This element is used by itself or immediately upstream of a centrifugal pump impeller in applications such as liquid-fuel rocket pumps, aircraft fuel pumps, and marine boiler pumps. The geometry of the inducer is characterized by a shallow-spiral angle (at the tip, 5 to 15 degrees from tangential) and (frequently) high-solidity, low aspect-ratio blades. These flow passages allow the time and space for the collapse of cavitation bubbles and a gradual head increase. However, the long passages of high aspect ratio lead to considerable viscous effects and strong secondary flows. In 1982, a review paper by Lakshminarayana (1982) included an extensive examination of inducer studies to that date, including his own program of internal flow measurements within rotating inducer passages, employing an air-flow model (see, for example, Lakshminarayana 1973). He identified four flow regions of interest in a blade-to-blade passage cross section. They were the core region, two wall boundary-layer regions with strong radial flows, and an "interference" region near the shroud. Recently Boccazzi *et al.* (1986, 1990) have presented internal velocity field measurements in a constant-spiral-angle inducer with low solidity.

The present investigation developed from a study, reported by Howard *et al.* (1987) and Abramian *et al.* (1988), that included measurements of the velocity field ahead of an inducer impeller and within the entry region of the rotating passages. The major fluid-flow phenomenon of interest there was the formation of entry tip stall and the consequent upstream swirling flow. This occurred at flow rates below design and is a feature observed in other forms of pump impellers and centrifugal compressors. The stall and reverse-flow region was observed only at the immediate entry region, even at the lowest flow rates.

The investigation described here used both laser-Doppler velocimetry (LDV) and traditional pressure probes to determine the flow field at the exit of the same inducer, both inside and outside the impeller passages. The exit casing was designed to provide circumferentially uniform conditions at all flow rates. The flow field was studied at design flow rate and at lower flows. The conditions in the exit region can be of particular importance to a designer, since they establish the level and distribution of energy transferred to the fluid. The tests were carried out for single-phase liquid flow, without cavitation effects.

Experimental apparatus and methods

Inducer test rig

The investigations were conducted in a water test facility arranged in a closed-loop circuit, as shown in Figure 1. A combination of a variable-speed boost pump and a butterfly valve allowed the flow through the circuit to be controlled. A large cylindrical chamber, referred to as a "dump," was substituted for the volute employed previously (Howard *et al.* 1987; Abramian *et al.* 1988) as the pump casing. The purpose was to realize an environment, at the inducer exit, with a uniform circumferential distribution of flow parameters at all flow rates. By avoiding the distortion usually caused by the volute at off-design flows, a measuring traverse at one circumferential location can represent the flow around the entire test cross section. Of course, the circumferential variation within the reference frame rotating with the impeller may be measured and constitutes a principal part of the data presented here.

Geometry and performance measurement methods

The design characteristics and geometry of the inducer are summarized in Table 1, while the inducer is shown in Figure

Address reprint requests to Professor Howard at the Mechanical Engineering Department, University of Waterloo, Waterloo, Ontario, Canada N2L 3G1.

Received 25 February 1992; accepted 5 June 1992

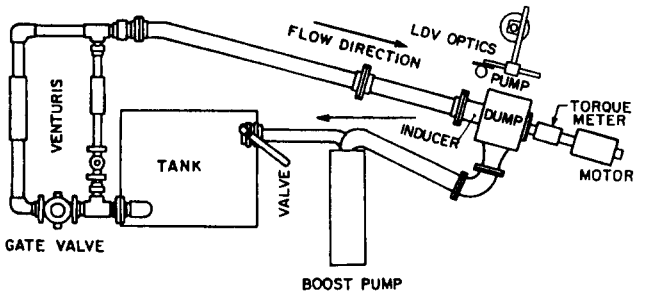

Figure 1 Experimental test loop—schematic

2. The introduction of variation in the blade angle through an inducer allows a higher head rise, but this must be accompanied by a sloped hub to limit diffusion in the impeller passage. In some cases a sloped hub is needed to match the downstream impeller. The blade angle is constant for the test inducer over an axial length corresponding to a tip solidity of one, then smoothly varied toward the exit. The angle was held constant at the exit over a distance corresponding to the "uncovered" portion of the passage. The geometry differs from the constant-spiral-angle, constant-hub diameter form, which was measured carefully by Boccazzi *et al.* (1986, 1990). The Boccazzi inducer also had a low solidity (1.0 at the tip) and was followed by a centrifugal impeller.

The inducer was operated at a constant speed of 1700 rpm, using a feedback speed control. Torque was measured by a rotary transformer torquemeter mounted between motor and inducer.

The head rise across the inducer was based on a traverse of the total head at 8 mm downstream of the inducer exit using a cobra probe. The differential pressure transducer measured the pressure head with respect to that in the tank. To this was added the pressure loss through the venturi and piping between the tank and inducer, calibrated as a function of flow rate. This approach avoided errors associated with a direct measurement of pressure upstream of the inducer, since at low flow rates, backflow from the inducer produces upstream swirl and a radial pressure gradient in the intake pipe. The flow rate was determined using a previously calibrated venturimeter. All measurements were time averaged.

LDV measurement technique

The LDV system employed for velocity measurements consisted of a 5W Argon-ion laser with single component transmitting and receiving optics arranged in backscatter mode. A single Bragg cell and electronic downmixing was used to provide the frequency shifting necessary to detect reverse flow. Two (axial and tangential) velocity components were obtained by rotating the optics. The optics block was mounted on a traversing mechanism installed vertically above the test section, as shown in Figure 3. Because of this arrangement, the use of an optical fiber was necessary to transmit the laser beam from the source to the optics. A window, made of flat Silica glass, was installed on the inducer housing for optical access, as illustrated in Figure 4.

The signal processor used for the task was a frequency counter. The digital output from the counter was read directly by a personal computer using a specially designed parallel interface. Two programs were used to process the velocity data. The first is a general-purpose measurement program that computes the mean and standard deviation of the local flow velocity. Using the program, point-by-point velocity profiles could be measured. The second program is used to compute velocities correlated with the angular position of the inducer shaft. The angular positions were obtained from an incremental angle encoder attached to the inducer shaft. Measurements were gathered in segments of 6 degrees each. Using this program, blade-to-blade velocity profiles could be obtained.

Small quantities of latex particles (1 μm nominal diameter) were used for seeding to improve the data rate.

Table 1 Inducer: geometry and design characteristics

Design flow rate	11.0396 L/s (175 gpm)
Design head	1.993 m (6.54 ft)
Design speed	1700 rpm
Tip diameter	127 mm (5 in)
Hub diameter—at inlet	38.1 mm (1.5 in)
—at exit	63.5 mm (2.5 in)
Radial tip clearance	0.635 mm (0.025 in)
Axial length	88.9 mm (3.5 in)
Number of blades	2
Solidity at tip	3
Blade thickness	3.18 mm (0.125 in)
Blade tip angle—at inlet	82.5 degrees
—at exit	77.77 degrees
Angle variation on line normal to hub	$\tan\beta = (r/R_t)\tan\beta_t$

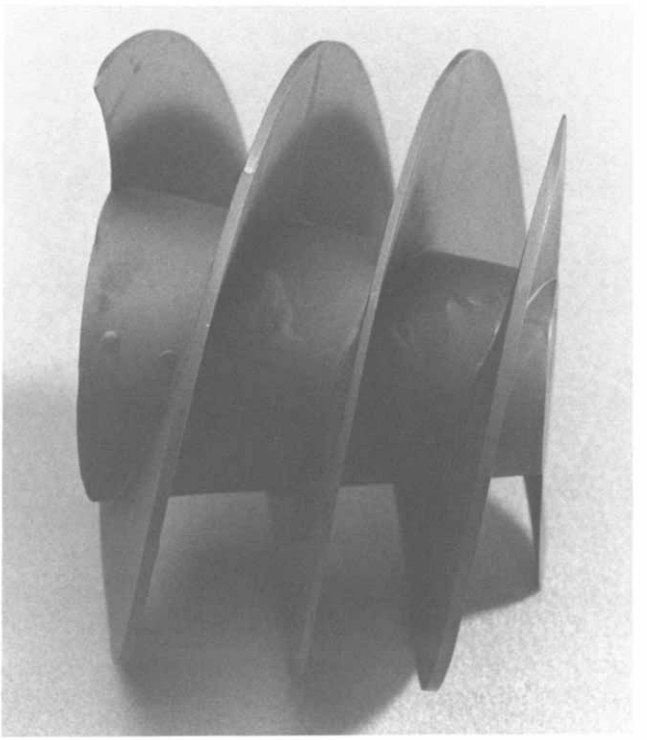

Figure 2 Inducer

Measurement accuracy

For the LDV system, measurement errors arise from the statistical uncertainty of the velocity measurement of any single particle and from averaging biases. Consideration of closely similar measurement conditions (see Howard *et al.* 1987) lead to the estimate that measurement accuracy was within ± 0.05 m/s. For the distributed velocities, further error can arise in regions with a high velocity gradient, where the averages over a 6-degree angle segment can be biased toward the higher velocities.

The average velocity distributions downstream of the inducer

were compared with measurements obtained with a cobra-probe traverse. On both measurement planes, the axial component velocities were integrated and compared with the measured flow rate. This latter procedure suffered from the necessity for extrapolation from the limited number of measurement radii, but the error was always less than 7 percent.

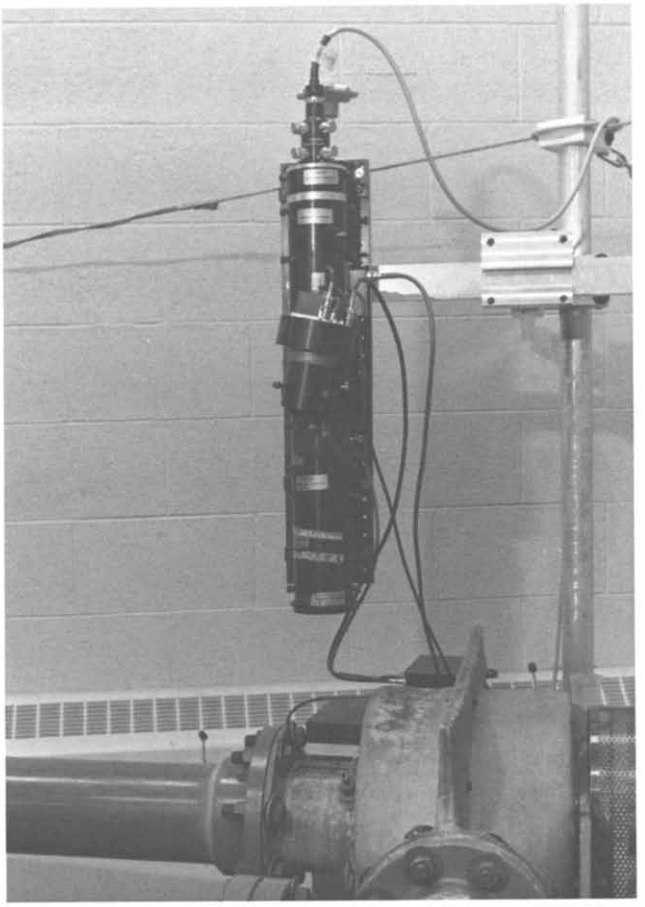

Figure 3 LDV measurement system—optics

Results and discussions

Measured performance

The characteristic curves from the performance investigation, presented in Figure 5, show trends typical of all axial-flow inducers. An early presentation and discussion of such performance is that by Anderson *et al.* (1964). In the present investigation, the maximum efficiency was 67.5 percent at a flow rate of 10.6 L/s. In contrast to some other studies, such as that of Anderson *et al.* (1964), the efficiency was based on measured torque, rather than from exit angular momentum calculated by the integration of downstream velocity measurements.

LDV measurements

Test conditions. Since the preliminary velocity measurements at the inducer exit (using traditional pressure probes) indicated a significant change in the flow field and some reverse flow as the flow rate was reduced, three flow rates were chosen for the LDV surveys: design flow rate and two lower flows. These are labeled Q_1, Q_2, and Q_3 and are marked on Figure 5 and detailed in Table 2. The flow rates were chosen to describe the observed

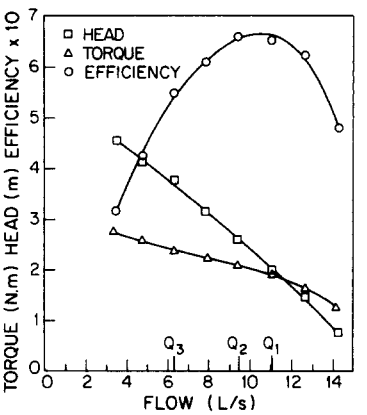

Figure 5 Inducer performance

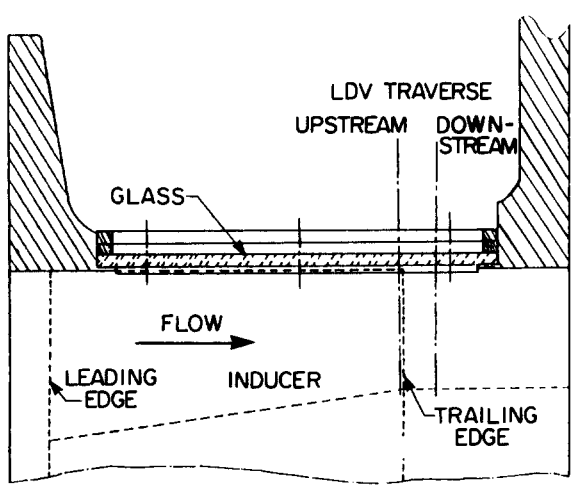

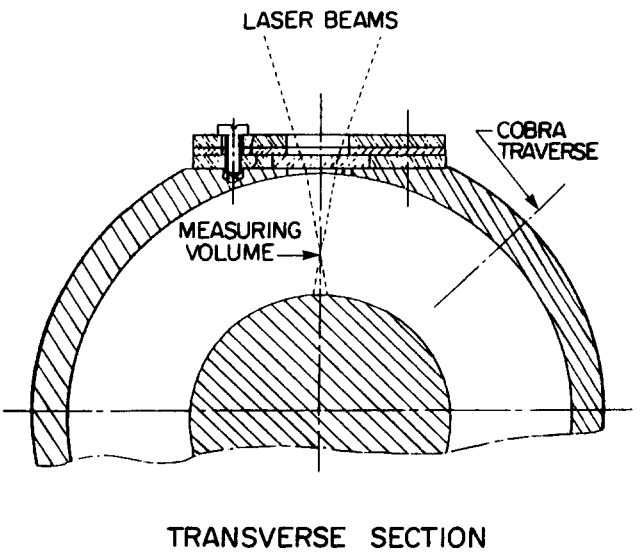

Figure 4 Optical window and measurement locations

Table 2 Flow rates for LDV traverse and pressure-probe measurements

Designation	Flow (L/s)	Flow (gpm)	% of design
q_1	14.27	226.21	129.3
q_2	12.68	201.00	114.9
Q_1	11.04	175.01	100.0
Q_2	9.45	149.80	85.6
q_5	7.87	124.76	71.3
Q_3	6.22	98.60	56.3
q_7	4.77	75.61	43.2
q_8	3.48	55.17	31.5

Note: Q: LDV and pressure probes; q: pressure probes only

Table 3 Radial measurement locations for full LDV traverse

Designation	Radius (mm)	Radius (in)	$(R-R_{hub})/(R_{tip}-R_{hub})$
R_1	34.29	1.35	0.08
R_2	40.64	1.60	0.28
R_3	46.99	1.85	0.48
R_4	53.34	2.10	0.68
R_5	59.69	2.35	0.88

development of the region of reverse flow near the hub at the inducer exit. For convenience, five radial locations, evenly spaced between hub and tip and listed in Table 3, were selected for the laser velocity traverses. No attempt was made to measure the velocity in the tip clearance region.

The LDV traverses were carried out at two axial stations. The upstream station is 1 mm from the trailing edge of the blades, i.e., inside the inducer, and the downstream station is 8 mm from the trailing edge, at the same location where earlier pressure-probe measurements were made. Figure 4 illustrates the measuring stations.

Measured velocity field. Figures 6a, 6b, and 6c present the circumferential distribution of the absolute velocity vector for the flow rates and radial locations investigated. At the upstream station, the blade locations can be easily recognized by zero-velocity measurements resulting from blades blocking the

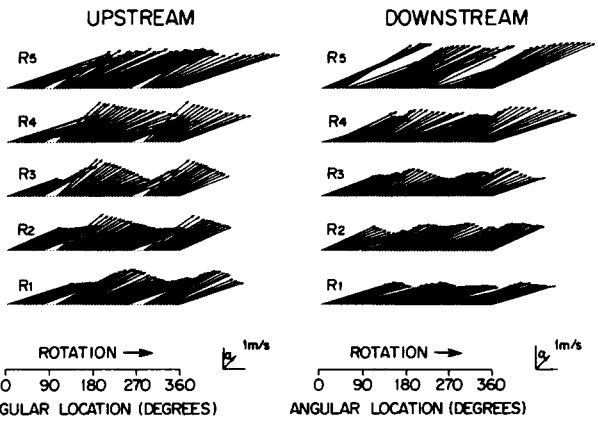

a

Figure 6(a) Absolute velocity vectors (combination of axial and tangential components) with design flow rate Q_1. Circumferential distribution is based on LDV traverse for two stations (upstream, downstream). Scale is shown on each portion of the figure by a sample vector of 1 m/s length. This also defines α, which is the angle between the vector and the axial direction

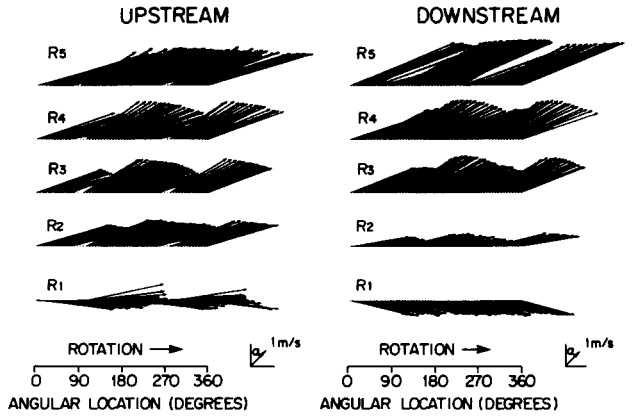

b

Figure 6(b) Absolute velocity vectors (combination of axial and tangential components) with flow rate Q_2. Circumferential distribution based on LDV traverse for two stations (upstream, downstream). Scale is shown on each portion of the figure by a sample vector of 1 m/s length. This also defines α, which is the angle between the vector and the axial direction

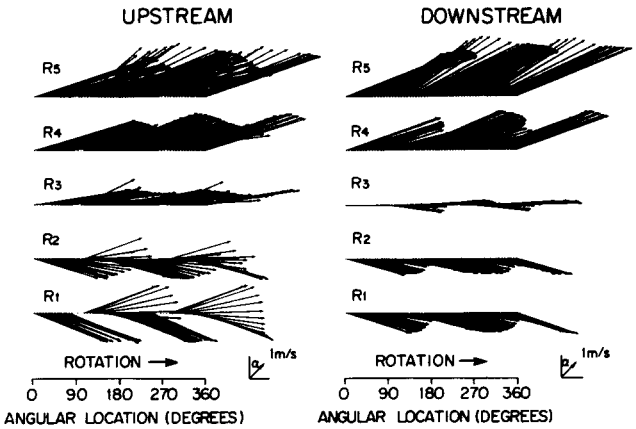

c

Figure 6(c) Absolute velocity vectors (combination of axial and tangential components) with flow rate Q_3. Circumferential distribution is based on LDV traverse for two stations (upstream, downstream). Scale is shown on each portion of the figure by a sample vector of 1 m/s length. This also defines α, which is the angle between the vector and the axial direction

laser beams. This form of data presentation allows comparison between flow rates and measurement locations, while presenting all data individually. However, certain features of the flow are more clearly shown by alternate plots.

Figure 7 presents the radial distribution of circumferentially averaged velocity components. Two techniques were employed at the downstream location. The "downstream traverse" was directly averaged by the LDV signal processor as outlined above and was carried out at a larger number of radial locations. The "average downstream" is a circumferential average of the data presented in Figures 6a, 6b, and 6c. This latter form of data is the only type available for the upstream location.

Design flow rate Q_1. At the upstream station, as shown in Figure 6a, the absolute velocity and flow angle vary moderately from blade to blade at the radius R_5 and more strongly near the hub. Figure 7 isolates the hub to shroud velocity variations. A reducing absolute tangential velocity with radius in the inner

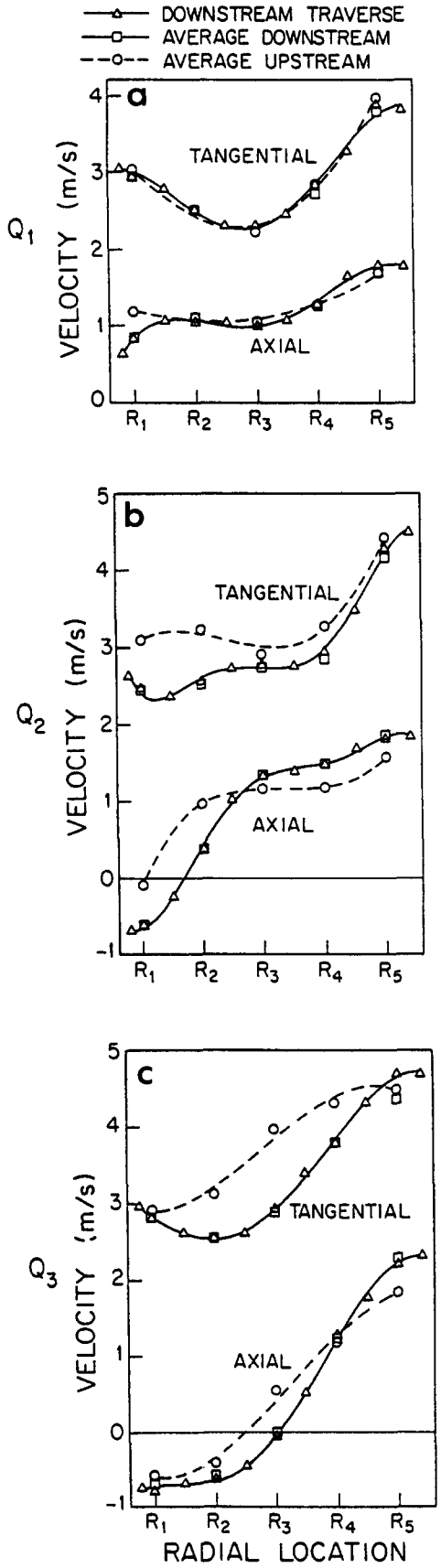

Figure 7 Distribution of circumferentially averaged absolute velocity based on LDV measurements for three flow rates. The downstream traverse is averaged by the LDV system

portion of the passage keeps the flow close to a free vortex, while from the midradius outward, the sharply increasing product of radius times tangential velocity leads to a sharp rise in Euler head. At the radius R_5, this head is more than double the value at the inner three-measurement radii. At the same time, an increase of axial velocity with radius shows that the flow is concentrated toward the tip. Minimum axial velocity and maximum absolute tangential velocity are found close to the suction side of the passage. The total relative velocity, formed by combining the axial and relative tangential components while ignoring the unmeasured radial component, is plotted in Figure 8. The relative velocity has its minimum close to the suction side, as may be expected in this region close to the passage exit as the blade unloads. The velocity minimum moves away from the wall at the outer two radii, which suggests the interaction of a secondary vortex with the radial transport of boundary-layer fluid toward the tip region as described by Lakshminarayana (1982). The secondary flow pattern is discussed in a separate section below.

Downstream, as shown in Figure 6a, the circumferential distribution of the flow field has become somewhat more uniform, even at this short distance from the trailing edge, while Figure 7 shows the radial distribution little altered except for the axial velocity component near the hub. Low axial and high (absolute) tangential velocity regions at the blade locations show the presence of wakes that are developing behind the blades. Results reported by Boccazzi *et al.* (1990) showed similar tangential velocity profiles at flow rates lower than design.

Reduced flow rate Q_2. When the flow is reduced, significant changes occur in the flow field. From Figures 6b and 7, for reduced flow rate Q_2 and at the upstream station, the new feature is the reverse flow developing near the hub. It is found over most of the hub passage except near the pressure side where some forward flow still persists. A similar result was reported by Boccazzi *et al.* (1990), although with a weaker recirculation zone. At other radii, the blade-to-blade distribution is the same as observed at the design flow rate.

Downstream, pure reverse flow is observed near the hub. The magnitude and uniform distribution suggests that such flow starts first downstream of the inducer due to considerable flow redistribution (Lakshminarayana 1973). The flow field is no longer symmetric and shows a recirculation pattern repeated at each blade passage. This pattern consists of reverse flow

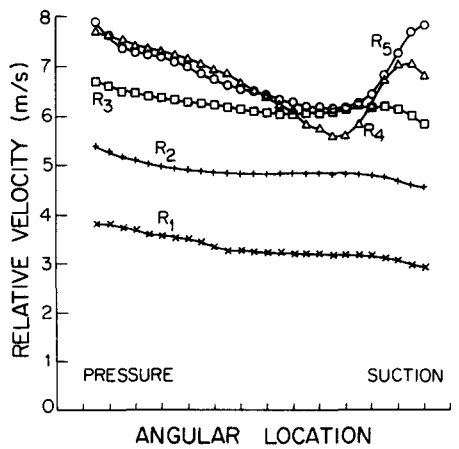

Figure 8 Distribution of relative velocity, ignoring the radial component, at upstream location and design flow rate Q_1

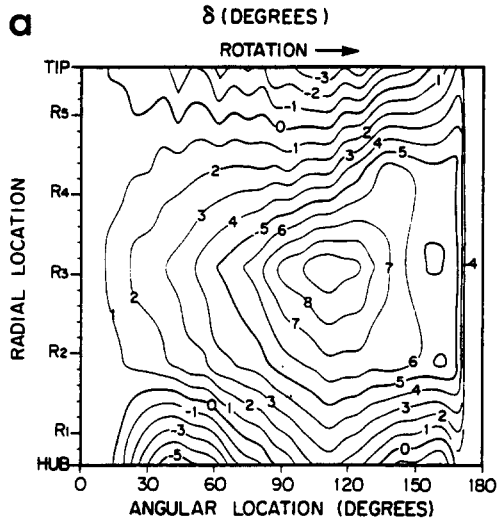

Figure 9(a) Deviation of the relative flow angle from the blade angle; distribution across the passage at the upstream location for design flow rate Q_1

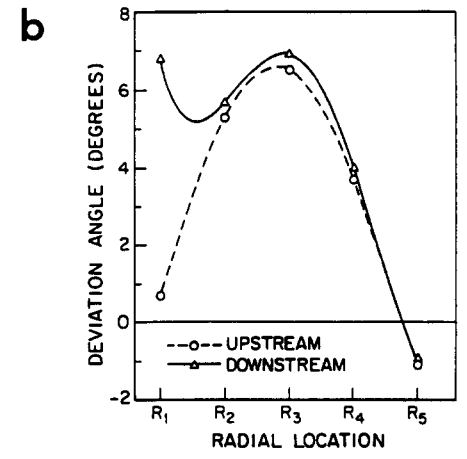

Figure 9(b) Radial distribution of the average deviation angle at design flow rate Q_1

entering the passage toward the suction side and exiting downstream in a concentrated region near the pressure surface. The wakes behind the blades are larger. The radial distribution of axial velocity (Figure 7) changes significantly from upstream to downstream. Reverse flow occurs over a much smaller radial extent upstream than downstream, suggesting that the exiting recirculation flow has a strong radial component. For the tangential velocity, the main flow redistribution occurs near the hub.

Reduced flow rate Q_3. As the flow is further reduced to Q_3, at the upstream location the extent of the reverse flow region grows further. From hub to mid-radius, as shown in Figure 6c, negative axial velocity occupies most of the blade passage except near the pressure side, where some strong forward flow remains, forming a strong blade-to-blade recirculation pattern. This is reflected at the downstream location by a strong circumferential gradient in the flow vector pattern. In addition, the downstream distribution shows a pure, strong reverse flow extending to midradius. The wakes behind the blades are wider.

From Figure 7, it may be seen that at flow Q_3, the downstream reverse flow near the hub tends to spread to larger radii rather than increasing in magnitude, which produces high velocities in the tip region even though the overall mean velocity is low.

Deviation angle. The deviation angle serves as a measure of the departure of the flow direction from that associated with perfect guidance by the blades, and is one form of representation of the secondary flow field. An accurate prediction of the deviation angle at the exit is also important in the design procedure. Figure 9a shows the distribution of the deviation angle across the upstream passage section at the design flow rate Q_1, while Figure 9b shows the circumferential average spanwise variation at both upstream and downstream. The overturning in the tip region contrasts with underturning observed in that region by Boccazzi *et al.* (1990). The present inducer also had a somewhat higher deviation at midradius. These differences are probably associated with the higher solidity of this machine and with its nonconstant pitch, which leads to a higher head rise at design flow.

The original design of this inducer had included the assumption of zero exit deviation (averaged at the mean radius). The measurements do not confirm this, since near-zero deviation occurs only close to the blades and near hub and tip. Maximum deviation is found at the center of the passage and rather closer to the suction side, while negative deviations are largely in the tip region. The pattern is consistent with a two-vortex secondary flow field. The radial distribution of the circumferentially averaged deviation angle, weighted to conserve angular momentum, shows a strong change in flow angle from upstream to downstream at the near-hub measurement radius, and little change elsewhere. Since the axial velocity and radius is lower near the hub, the angular-momentum change associated with the deviation-angle change near the hub is small. A similar angular distribution, based on downstream measurements with a pressure probe, was reported by Sandercock *et al.* (1962).

A common preliminary design procedure involves flow predictions at the root-mean-square radius at the impeller outlet. The measured mean deviation angle at that radius was found by integrating the angular momentum across the passage. The deviation angle that generated the same angular momentum from the mean axial velocity was 3.56 degrees based on the upstream location and 4.15 degrees based on downstream measurements (both at design flow Q_1). At flow rate Q_2, the mean deviations were 4.19 degrees (upstream) and 4.33 degrees (downstream). The deviations at flow rate Q_3 were 4.72 degrees and 4.76 degrees for upstream and downstream, respectively. The increase in deviation angle downstream is consistent with constant angular momentum between the two stations, within the accuracy of the integration methods, because of the blade blockage effects at the upstream station. Further presentation of the distribution of deviation angle is included by Atif (1991).

Secondary flow pattern

Secondary velocity is defined as that component lying on a plane normal to the mean passage direction. Although the blade-to-blade traverses are in the circumferential direction, the secondary velocity may be determined at each measurement point by combining the appropriate components of the axial and relative tangential velocities. Since the radial component is not measured, a vector-style presentation of the secondary flow field is not useful. Much of the general characteristics of the secondary velocity distribution is shown by the deviation-angle distribution, Figure 9a. In Figure 10, several strong features of the secondary flow are revealed by the

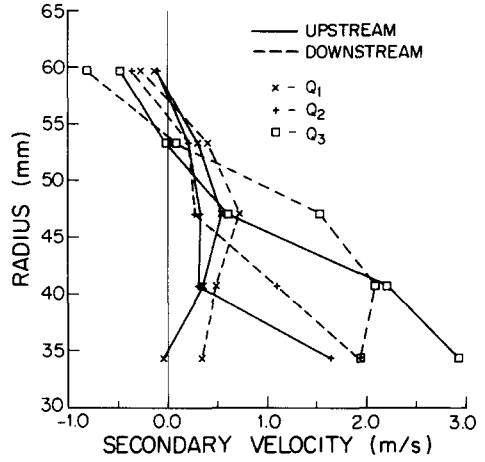

Figure 10 Circumferentially averaged radial distribution of secondary velocity for three flow rates. Secondary velocity is the component of relative velocity normal to the passage direction. Solid line: upstream. Dashed line: downstream

distribution of the circumferentially averaged secondary velocity. As noted above, a principal secondary flow feature is the presence of two large secondary vortices with opposite rotation, for flow Q_1. This is borne out by the radial gradient of the secondary velocity. At the downstream location, the tip region vortex has strengthened, while that at the hub region has weakened slightly. This flow pattern is similar to that in other high-solidity turbomachinery passages, such as centrifugal impellers, and is somewhat less complex than that suggested by Lakshminarayana (1982). At the lower flow rates, the reverse axial flow wipes out or reverses the hub vortex, while the tip vortex increases modestly.

Pressure-probe velocity measurements

The axial and tangential velocity components, obtained at the downstream location using the cobra probe, are presented in Figure 11. The axial velocity component is directly compared to LDV data taken from Figure 7 and can be seen to be closely similar. The tangential component data are not directly compared on the plot to avoid clutter. It is also similar, but not as close as is the case for the axial component data. This serves both to confirm the different measurement methods and to uphold the achievement of circumferential uniformity, since the traverse locations were separated by 45 degrees. The wider range of flow rates (see Table 2) shows the continuous development (with lowering flow rate) of the hub reverse flow and high tip velocities. The head is observed to rise toward the tip, but not as rapidly as the Euler head discussed above, confirming the expected high losses in the tip region (Lakshminarayana 1982).

Flow pattern in the meridional plane

When the velocity field near the inducer entrance (see Howard *et al.* 1987; Abramian *et al.* 1988) is combined with the present data, an overall pattern of flow in the meridional field is suggested. At the design flow rate, the streamlines will move toward the outer radius as the flow progresses from entry to exit. At lower flow rates, reverse flows appear at the entry tip and the exit hub. Figure 12 portrays the expected streamline pattern in the meridional plane at flow rate Q_3. The cross-hatched sections are regions where reverse axial velocity was observed.

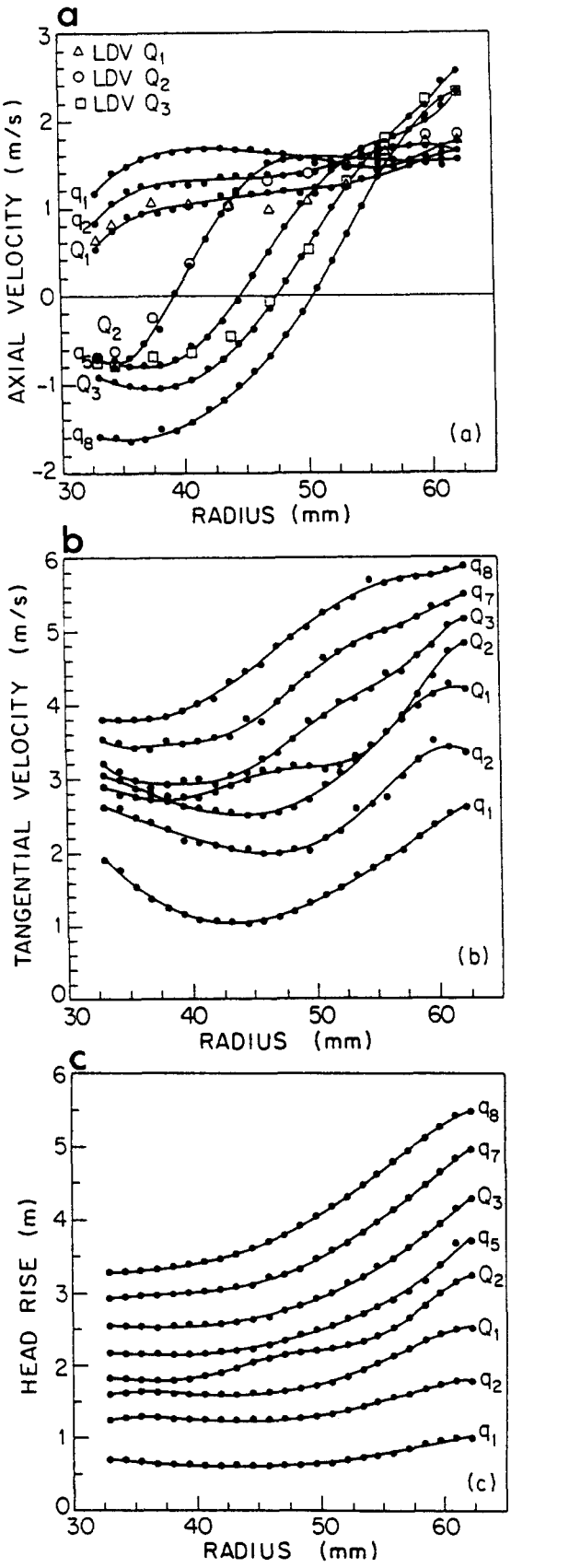

Figure 11 Radial distribution of downstream velocity components and head rise based on cobra-probe measurements and comparisons with LDV data (axial component only)

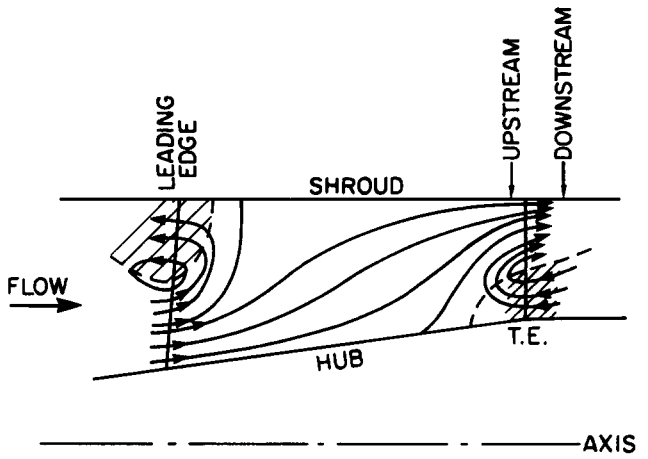

Figure 12 Flow pattern in the meridional plane at flow Q_3, as suggested by data and by Howard *et al.* (1987) and Abramian *et al.* (1988)

Conclusions

The velocity field at the exit of a high-solidity spiral inducer has been measured both within the rotating passage and immediately downstream. Together with earlier measurements near the entry of this inducer, this represents a complete definition of the impeller flow field over a range of flow rates. This low aspect ratio, high-solidity geometry produces a complex three-dimensional flow, which at the design flow rate may be characterized by a two-vortex secondary flow pattern.

The performance characteristics of the inducer were representative of this type of machine. However, comparison of the detailed velocity distribution with data from a low-solidity, constant-spiral-angle inducer mounted ahead of a centrifugal impeller showed variations in tip deviation angle and secondary flow pattern. The exit flow pattern appears to vary with solidity, design head rise, and possibly the passage geometry downstream of the inducer.

The data reveal a rearrangement of the flow field between measurement locations upstream and downstream of the trailing edge, even though the stations were very close. Most of the changes are near the hub. Furthermore, when the flow is reduced, the velocity field becomes increasingly distorted, with reverse flow at the hub. A recirculation region near the hub forms and expands when the flow is further reduced. The recirculating flow enters the passage toward the suction side and exits in a narrow region at the pressure side with added radial velocity. The resultant blockage produces high velocities in the tip region.

Acknowledgments

The research described here was supported by a grant from the Natural Sciences and Engineering Research Council of Canada. The second author was supported by the Ministry of Higher Education of Algeria and the Canadian International Development Agency.

References

Abramian, M., Howard, J. H. G. and Hermann, P. 1988. An investigation of axial pump backflow and a method for its control. ASME paper 88-GT-31

Anderson, D. A., Soltis, R. F. and Sandercock, D. M. 1964. Performance of 84° flat-plate helical inducer and comparison with performance of similar 78° and 80.6° inducers. NASA TN D-2553

Atif, A. 1991. Performance evaluation and near-exit flow field investigation in an inducer pump. M.A.Sc. thesis, Department of Mechanical Engineering, University of Waterloo

Boccazzi, A., Coghe, A. and Perdichizzi, A. 1986. LDA measurements on the inducer of a centrifugal pump. Third Int. Symp. Appl. Laser Anemometry Fluid Mech., Lisbon, July 7–9, 1986

Boccazzi, A., Perdichizzi, A. and Tabacco, U. 1990. Flow field investigation in a low-solidity inducer by laser-Doppler velocimetry. *ASME J. Turbomach.*, **112**, 91–97

Howard, J. H. G., Tropea, C., Almahroos, H. M. H. and Roeber, T. W. 1987. LDA measurements of the velocity field within and ahead of an axial pump inducer at off-design flow rate. *Proc. 1987 ASME/JSME Thermal Eng. Joint Conf.*, **2**, 63–69

Lakshminarayana, B. 1973. Three-dimensional flow field in rocket pump inducers., part 1: measured flow field inside the rotating blade passage and at the exit. *ASME J. Fluids Eng.* **95**, 567–578

Lakshminarayana, B. 1982. Fluid dynamics of inducers—a review. *ASME J. Fluids Eng.*, **104**, 411–427

Sandercock, D. M., Soltis, R. F. and Anderson, D. A. 1962. Cavitation and non-cavitation performance of an 80.6° flat-plate helical inducer at three rotational speeds. *NASA*, TN D-1439